Ultrasensitive immunoprofiling of plasma extracellular vesicles identifies syndecan-1 as a potential tool for minimally invasive diagnosis of glioma

Vineesh Indira Chandran[1], Charlotte Welinder[1,2], Ann-Sofie Månsson[1], Svenja Offer[1], Eva Freyhult[3], Maria Pernemalm[4], Sigrid M. Lund[5], Shona Pedersen[5,6], Janne Lehtiö[4], Gyorgy Marko-Varga[2,7], Maria C. Johansson[1], Elisabet Englund[1], Pia C. Sundgren[8,9,10], Mattias Belting[1,11,12*]

[1]Department of Clinical Sciences, Lund, Section of Oncology and Pathology, Lund University, Sweden; [2]Center of Excellence in Biological and Medical Mass Spectrometry (CEBMMS), Lund University, Sweden; [3]National Bioinformatics Infrastructure, SciLife Lab, Uppsala, Sweden; [4]Department of Oncology and Pathology, Karolinska Institute, Sweden; [5]Department of Clinical Biochemistry, Aalborg University Hospital, Denmark; [6]Faculty of Clinical Medicine, Aalborg University, Denmark; [7]Clinical Protein Science & Imaging, Biomedical Center, Department of Biomedical Engineering, Lund University, Sweden; [8]Department of Clinical Sciences, Lund, Section of Diagnostic Radiology, Lund University, Sweden; [9]Lund BioImaging Centre, Lund University, Sweden; [10]Department of Medical Imaging and Function, Skåne University Hospital, Lund, Sweden; [11]Department of Hematology, Oncology and Radiophysics, Skåne University Hospital, Lund, Sweden; [12]Department of Immunology, Genetics and Pathology, Uppsala University, Sweden.

***To whom correspondence should be addressed:** Mattias Belting, Department of Clinical Sciences, Lund, Section of Oncology and Pathology, Lund University, Barngatan 4, SE-221 85, Lund, Sweden; Tel: +46-46-178549; E-mail: mattias.belting@med.lu.se

Running title: *Extracellular vesicle liquid biopsy for brain tumor diagnosis.*

Key words: *Glioma, liquid biopsy, extracellular vesicles, proteomics, syndecan-1.*

Additional information

Financial support: This study was funded by grants from the Swedish Cancer Fund CAN 2017/664 and 2016/365 (M.B. and P.C.S.); the Swedish Research Council VR-MH 2014-3421 and K2011-52X-21737-01-3 (M.B. and P.C.S.); the Swedish Childhood Cancer Foundation PR2015-0078 (M.B.); the Gunnar Nilsson Cancer Foundation; the Fru Berta Kamprad Foundations (M.B.); the Skåne University Hospital donation funds (M.B.); the Governmental funding of clinical research within the national health services, ALF (M.B. and P.C.S.); EU Horizon 2020 AiPBAND MSCA-ITN-ETN (M.P. and J.L.); and a donation by Viveca Jeppsson (M.B.).

Conflicts of interest: The authors have no conflicts of interest to declare.

Word count (excluding figure legends & references): 5287

Number of Figures and Tables: 6

Supplementary Figures: 4

Supplementary Tables: 2

Supplementary Data Files: 2

Translational relevance

The development of non-invasive strategies for brain tumor diagnosis remains a challenge of high clinical relevance. Extracellular vesicles (EVs) have received considerable attention as a potential liquid biopsy biomarker as they represent "a miniature of its cell of origin". Here, using an interdisciplinary approach, we have developed a new procedure for the isolation and analysis of patient plasma EVs. In a well-defined glioma patient study cohort, we for the first time identify syndecan-1 (SDC1) as a EV constituent that non-invasively can discriminate between GBM (WHO grade IV) and low grade glioma (WHO grade II). Importantly, we found strong support of EV-SDC1 originating directly from GBM tumors. We conclude that tumor-derived EVs may serve as a potential tool to facilitate minimally invasive diagnosis and monitoring of gliomas, which should stimulate future efforts to move this field closer to the goal of improving the management of cancer patients.

Abstract

Purpose: Liquid biopsy has great potential to improve the management of brain tumor patients at high risk of surgery-associated complications. Here, the aim was to explore plasma extracellular vesicle (plEV) immunoprofiling as a tool for non-invasive diagnosis of glioma. **Experimental design:** PlEV isolation and analysis were optimized using advanced mass spectrometry, nanoparticle tracking analysis and electron microscopy. We then established a new procedure that combines size exclusion chromatography isolation and proximity extension assay (PEA)-based, ultrasensitive immunoprofiling of plEV proteins that was applied on a well-defined glioma study cohort (*n*=82). **Results:** Among potential candidates, we for the first time identify syndecan-1 (SDC1) as a plEV constituent that can discriminate between high grade glioblastoma multiforme (GBM, WHO grade IV) and low grade glioma (LGG, WHO grade II) (AUC: 0.81; sensitivity: 71%; specificity: 91%). These findings were independently validated by ELISA. Tumor SDC1 mRNA expression similarly discriminated between GBM and LGG in an independent glioma patient population from The Cancer Genome Atlas cohort (AUC: 0.91; sensitivity: 79%; specificity: 91%). In experimental studies with GBM cells, we show that SDC1 is efficiently sorted to secreted EVs. Importantly, we found strong support of $plEV^{SDC1}$ originating from GBM tumors, as $plEV^{SDC1}$ correlated with SDC1 protein expression in matched patient tumors, and $plEV^{SDC1}$ was decreased post-operatively depending on extent of surgery. **Conclusion:** Our studies support the concept of circulating plEVs as a tool for non-invasive diagnosis and monitoring of gliomas, and should move this field closer to the goal of improving the management of cancer patients.

Introduction

Primary brain tumors remain among the most challenging forms of cancer to diagnose and treat in adults and children. The World Health Organization uses histologic criteria to discriminate between low-grade (I and II) glial tumors with a relatively good prognosis, and high-grade tumors (III and IV, or glioblastoma multiforme, GBM), which are the most common and aggressive primary brain tumors in adults (1, 2). These molecular classifications are currently dependent on tissue samples obtained after biopsy or tumor resection. However, this is not always feasible, as intracranial tumors are among the most inaccessible for a diagnostic biopsy due to considerable risks of post-surgical complications (*e.g.* neurological damage, bleeding, infections), resulting in delayed onset of oncological treatment and ultimately worse patient outcome. The development of non-invasive strategies for the diagnosis of glioma tumors thus remains a challenge of high clinical relevance, especially with regard to tumor spatiotemporal heterogeneity (3).

Extracellular vesicles (EVs) are small (~40–1000 nm), lipid bilayer-enclosed vesicles secreted into a variety of biological fluids, including plasma. EVs have emerged as critical components in intercellular communication during the development and progression of cancer (4-7). The comprehensive molecular content of EVs, including proteins, RNA, DNA, and lipids, largely mimics their cell or tissue of origin, and tumor cells in general secrete excessive amounts of EVs. This has stimulated considerable efforts to develop EVs as a tool for minimally invasive diagnosis of cancer (8, 9). In GBM, a pilot study from our group suggested that the plasma EV (plEV) proteome reflects the tumor oxygenation status (10), whereas others have shown that serum and cerebrospinal fluid derived EVs correlate with EGFR expression and mutation status, tumor size, and treatment response (11-18). Although these studies are based on relatively small patient cohorts, they provide important support to the concept that EVs reflect the molecular profile of GBM tumors and can differentiate between GBM patients and

healthy control subjects; however, the need of discriminating between benign and malignant gliomas of different grades, which would have more obvious clinical impact, remains unmet.

To reach the full potential of EVs as a source of biomarkers and to distinguish plEVs from contaminating plasma proteins (19, 20), it is essential to identify specific tumor-derived EV proteins to facilitate down-stream, multi-omics profiling studies. Motivated by clinical needs, we have employed size exclusion chromatography (SEC), advanced mass spectrometry and an ultrasensitive proximity extension immunoassay in a well-defined population cohort of brain tumor patients in the search for tumor-derived plEV proteins.

Materials and Methods

A detailed description of LC-MS/MS experiments is given in *Supplementary Materials and Methods*.

Study design and sample collection

The patient material was from a population based trial cohort ("MRI study") encompassing patients referred to the Neurosurgery Department at Lund University Hospital, Lund, Sweden, with a suspicion of an intracranial tumor. Inclusion criteria were age 18 years or above, WHO performance status 0-3, and ability to give written informed consent before study entry. The study was carried out according to the ICH/GCP guidelines and in agreement with the Helsinki declaration, and was approved by the local ethics committee, Lund University (Dnr. 2011/814, and 2012/188). Patients were diagnosed by routine MRI of the brain (3T Magnetom Skyra, Siemens AG, Erlangen, Germany), surgical and pathological procedures, received standard oncological treatment and were followed up according to local and national recommendations as well as by repeated MRI examinations according to the study protocol including sagittal T1-w, axial T2-w, axial diffusion weighted imaging (DWI), axial and coronal T1-w ± gadolinium. Blood samples were collected in EDTA tubes, centrifuged at 2000x*g* for 10 min at RT and stored in a -80^{0}C freezer. Longitudinal plasma samples were collected at baseline (pre-operative) and 3 weeks after surgery (post-operative) prior to start of oncological treatment. The present biomarker cohort was established at the cut-off date of September 1st 2016, consisting of the first consecutive 136 patients. Before processing the clinical cohort, we performed extensive optimization of plEV isolation by SEC from control subjects at the Department of Oncology, Lund University. We validated the suitability of the plEV isolation techniques and its downstream processing in identifying potential EV protein biomarkers by conducting in-depth proteomic analyses using advanced LC-MS/MS (**Fig. 1**). Unblinding of clinicopathological parameters and corresponding experimental data was done after finishing all experiments.

Cell-lines

U87-MG GBM cells were purchased from ATCC, and routinely cultured in DMEM growth medium, supplemented with 10% foetal bovine serum (FBS), 2 mM L-glutamine, 100 U/ml penicillin and 100 μg/ml streptomycin (PEST). The U3043 cells are part of the Uppsala University Human Glioma Cell Culture resource (HGCC, www.hgcc.se) of patient-derived GBM cells, and were cultured on laminin in serum-free medium supplemented with EGF, FGF, and stem cell supplements, as previously described (35). Primary HBMECs were purchased from 3H Biomedical, and cultured in Endothelial culture medium (EC medium) (3H Biomedical) supplemented with 5% FBS, 1% EC growth supplement and 1% PEST. HBMECs at passages 2–4 were used for experiments. All cells were normally kept at 37^{o}C in a humidified 5% CO_2 incubator.

EV isolation

EVs were isolated from U87-MG cells by differential ultracentrifugation, as previously described (10). Briefly, sub-confluent cells were grown in serum-free DMEM supplemented with 1% BSA at normoxic or hypoxic conditions for 48 h, and conditioned media were collected and centrifuged at 300*g* twice to eliminate cell debris. Supernatant fractions were then centrifuged at 100,000*g* for 2 h to pellet EVs, followed by washing twice with PBS at 100,000*g* for 2 h.

For the isolation of EVs from plasma samples, sepharose-based CL-2B SEC columns (IZON Science) were employed. Plasma samples were thawed on ice for the first time after freezing. Five hundred μl plasma aliquots were applied to the column and 15 fractions of 500 μl were collected immediately with 2 mM $CaCl_2$ in PBS as the elution buffer. Fractions 5-9, corresponding to the EV elution profile, were pooled and lyzed by 10 cycles of free-thaw, with each cycle of freezing (15 min on dry ice), followed by thawing (3 min in an ultrasonic bath). Lyzed EV proteins were desalted using PD-10 columns (GE Healthcare) according to

the standard protocol. Purified EV proteins were concentrated by freeze-drying using Mini Lyotrap (LTE Scientific) and stored at -80^{o}C until further use.

EV processing for LC-MS/MS

Lyzed EVs in 6 M Urea/50 mM ammonium bicarbonate were reduced with 10 mM dithiothreitol (DTT) for 1 h at 56^{o}C with gentle shaking and alkylated using 50 mM iodoacetamide (IAA) for 30 min in the dark at room temperature (RT). Thereafter, protein samples were digested with sequencing grade trypsin (Promega) overnight at 37^{o}C with gentle shaking. The digestion was stopped by adding 2% trifluoroacetic acid (TFA) (1:10 v/v) and the samples were dried in a SpeedVac. Subsequently, they were either stored at -80^{o}C or resuspended in 0.1% TFA for further analysis.

LC-MS/MS, Normal Gradient (NG), Long Gradient (LG), and Tandem Mass Tag (TMT) labelling and High Resolution Isoelectric Focusing, HiRIEF was performed as described in *Supplementary Materials and Methods*.

Nanoparticle Tracking Analysis (NTA)

NTA was applied to determine the size and concentration of particles and to confirm that their size was equivalent to that of EVs (52). Particles were tracked on an LM10-HS system with a 405 nm laser (Malvern Instruments, Malvern, UK) and visualized with a Luca-DL EMCCD camera (Andor Technology, Belfast, UK). Standard silica beads (0.1-µm) were used to calibrate the analysis settings with a camera level of 10 and detection threshold 2 with blur 9×9. A total of five videos each of 30 s were recorded for the individual samples. Prior to analysis, the samples were diluted in PBS to ensure a particles/frame count within the manufacturers recommendations. Particles were tracked, quantitated, and size enumerated using the Nanosight NTA software version 3.0 (Malvern Instruments, Malvern, UK).

Transmission Electron Microscopy (TEM)

Approximately 5 µl of isolated EVs were adsorbed onto 400-mesh carbon coated gold grids. The dried samples were blocked with 1% BSA and incubated with anti-SDC1 rabbit monoclonal antibody (1:1000) (ab128936, Abcam) for 1 h at RT. After washing, samples were incubated with 10-nm gold-conjugated anti-rabbit secondary antibody (1:20) (15726, TED Pella Inc.). Control samples were incubated with only secondary antibody. Subsequently, the samples were fixed with 1% glutaraldehyde, stained with 2% uranylacetate and examined in FEI Tecnai BioTWIN TEM operated at an accelerating voltage of 100 KV. Images were recorded with an Olympus SIS Veleta CCD camera.

ProSeek Multiplex Proximity Extension Assay (PEA)

EV protein was analyzed using the Proseek Multiplex Oncology II^{96x96} and CVD III^{96x96} panels (Olink Bioscience), as previously described (26, 27). The protein quantification is based on proximity extension assay (PEA) technology, which provides high sensitivity and specificity based on the binding of oligonucleotide-labelled antibody probe pairs to their specific target protein, generating a PCR-amplified DNA template, which is proportional to the initial antigen concentration as quantified by real-time qPCR. Four internal and three negative controls were used to calculate the lower limit of detection (LOD) for each protein.

SDC1 ELISA

SDC1 levels in plEV samples were analyzed using the Human SDC1 ELISA Kit (Thermo Scientific) according to manufacturer´s instructions. Briefly, 100 µl of each standard and sample were added to appropriate wells and incubated for 2.5 h at RT with gentle shaking. After washing, 100 µl of 1× biotinylated antibody was added and incubated for 1 h at RT. Following another wash, 100 µl of Streptavidin-HRP solution was added to each well and incubated for 45 min at RT. One hundred µl of TMB substrate was then added to samples for 30 min at RT in the dark with gentle shaking, followed by the addition of 50 µl of stop

solution. The absorbance was measured at 450 nm and 550 nm in a spectrophotometer (FLUOstar OPTIMA).

Migration Assay

HBMECs were starved overnight in serum-free endothelial cell culture medium supplemented with 1% L-Glut and 1% PEST. Cells were added in serum-free medium to the top chamber of 8-µm pore cell culture inserts (BD Biosciences) placed in a 24-well plate. Cells were incubated for 6 h at 37°C to allow cell migration towards serum-free medium supplemented with plEVs isolated from patients or healthy controls (1.5 µg/ml) or serum-free medium with no additions. Migrated cells attached to bottom membrane were fixed with 4% (w/v) paraformaldehyde, stained with crystal violet, and counted from pictures taken under the microscope (Axiovert 40C, 4× objective; Carl Zeiss).

Immunoblotting

EV protein extracts were mixed with NuPAGE 4× LDS Sample Buffer (Life Technologies) and heated for 10 min at 80^{o}C. Proteins were resolved in a NuPage 4–12% Bis Tris gel (Life Technologies) at reducing conditions, and then transferred onto a polyvinylidene fluoride (PVDF) membrane (Immobilon-FL), followed by blocking in TBS containing 0.05% Tween-20, 5% nonfat dry milk for 1 h at RT. To probe for SDC1, the membrane was incubated with rabbit monoclonal anti-SDC1 (1:10,000) (ab128936, Abcam) in TBS 0.05% Tween 20 containing 5% nonfat dry milk overnight at 4^{o}C. After washing, the membrane was incubated with HRP-conjugated anti-rabbit secondary antibody (1:3000) (7074, Cell Signaling Technology). Protein bands were visualized by enhanced chemiluminescence western blotting substrate (Pierce).

Immunofluorescence

Cells were seeded on 4-chamber well slides (10,000 cells/well) overnight, fixed with 4% (w/v) paraformaldehyde for 10 min and permeabilized with 0.5% Saponin/PBS for 15 min at

RT. After washing, cells were incubated with rabbit monoclonal anti-SDC1 (ab128936, Abcam) (dilution 2 µg/ml) for 1 h at RT. After further washing, cells were incubated with AF-546-conjugated goat anti-rabbit secondary antibody (A11010, Life Technologies) (dilution 2 µg/ml) for 1 h in PBS/1% BSA in the dark for 10 min at RT. Control cells were stained with secondary antibody only. Cell nuclei were counterstained with Hoechst (1:20,000). Cells were analyzed using Zeiss LSM 710 confocal scanning equipment with a Plan-Apochromat20x/0.8 objective or a C-Apochromat 63x/1.2 W Korr objective and Zen software.

Immunohistochemistry (IHC)

IHC staining for SDC1 was performed on an automated IHC staining platform (Ventana Medical Systems, Roche) according to manufacturer´s instructions. Briefly, tissue was fixed with 4% formaldehyde, dehydrated, and paraffin embedded. Following deparaffinization, antigen retrieval was performed by treatment in Cell Conditioning solution (CC1, 950-124, Ventana Medical Systems, Roche) for 1 h at 95°C. Sections were then stained with mouse anti-human SDC1 antibody (B-A38; 760-4248, Ventana Medical Systems, Roche) for 50 min at 36°C, followed by visualization using 3,3′-Diaminobenzidine (DAB) Ultraview (Ventana Medical Systems, Roche) according to manufacturer's instructions.

Statistical analyses

Functional enriched pathway analyses of proteins were performed using ConsensusPathDB-human interaction network database (http://cpdb.molgen.mpg.de/). GBM WHO grade IV and LGG (astrocytoma grade II) RNA-Seq data for survival were downloaded from the TCGA data portal (https://tcga-data.nci.nih.gov/docs/publications/tcga/) as per recommended network instructions. The TCGA RNA-Seq data set for SDC1 expression was analyzed using data from the cBioPortal (http://www.cbioportal.org/). The TCGA GBM RNA-seq data sets for SDC1 expression in IDH wild type and mutant; tumor subtypes; and gene correlations (r-value) were analyzed using data obtained from the GlioVis portal

(http://gliovis.bioinfo.cnio.es/). In the PEA analysis, protein levels were expressed as Normalized Protein eXpression (NPX) values, an arbitrary unit on $\log_2$-scale. The LOD for a protein is computed based on blank samples as three times the standard deviation above the mean. The association between a protein NPX value and patient group (GBM or LGG) was investigated using linear regression, adjusting for age (there was no significant association between gender and group), and assessed using a likelihood ratio test. The linear regression approach was applied to all proteins with less than 20% values below LOD and all samples with a value below LOD were excluded in the analysis. Proteins with 80% or more values below LOD were excluded from the analyses. Proteins with 20% or more values below LOD (but less than 80%) were discretized (coded as 0=below LOD, 1=above LOD). The association between a discretized protein variable was estimated using logistic regression, adjusting for age and using a likelihood ratio test, as for the linear regressions described above. The association of $plEV^{SDC1}$ and $plEV^{ITGB2}$ expression with glioma grade (GBM WHO grade IV and LGG/astrocytoma WHO grade II) was calculated using unpaired two-tailed Student´s *t*-test. Associations between $plEV^{SDC1}$ and $plEV^{ITGB2}$ expression and GBM patient survival were analyzed using Log-rank (Mantel-Cox) Chi-squared test. ROC curves were used to determine the specificity and sensitivity, and were expressed as area under the ROC curve (AUC). The cutoff points were selected using Youden's index, which maximizes the sum of sensitivity and specificity. Group differences involving GBM subtypes were tested by Simple one-way ANOVA test. In the PEA analyses, P-values were adjusted for multiple tests using Benjamini-Hochberg's method for controlling the false discovery rate (FDR<0.05). $P<0.05$ was considered statistically significant. Data are presented as the means $\pm$ SD. All figures were prepared and analyzed using either GraphPad Prism version 7.0 (GraphPad Software) or in R version 3.4.2.

Results

Optimization of EV isolation from patient plasma

To optimize procedures for the isolation of EVs from patient plasma, we initially compared well-established centrifugation procedures for *in vitro* isolation of glioma cell-derived EVs (gcEVs) (10, 21) with SEC-based isolation of plEVs from patients (**Fig. 1A**). The distribution of total protein and particles in separate SEC fractions (15 fractions were collected) was assessed by gel electrophoresis and nanoparticle tracking analysis, revealing that the bulk of plasma proteins gradually increases from fraction 10 (**Fig. 1B)**, and that the particle concentration peaked in SEC fraction 9 (**Fig. 1C**). This is consistent with the typical elution pattern of EVs from sephadex-based SEC columns with a pore size of approximately 75 nm (19, 22, 23). Nanoparticle tracking analysis of gcEVs (**Fig. 1D**) and plEVs from SEC fractions 5-9 (**Fig. 1E**), showed comparable size distributions with a median particle size of approximately 130 and 110 nm, respectively. Electron microscopy (EM) studies corroborated these data, showing similar size distribution and morphology of gcEVs and plEVs (**Fig. 1F** and **G**). The composition of plEVs was initially determined by normal gradient shotgun LC-MS/MS proteomics and compared to the gcEV proteome (**Fig. 1H** and **Data File S1**). We found 328 overlapping protein identities, and there was expectedly high coverage for abundant plasma proteins such as complement factors, coagulation factors, and apolipoproteins in plEV isolates (**Data File S1**). With the aim of improving the detection of low abundant plEV proteins, we employed a long gradient LC-MS/MS approach that increased the overlap with gcEVs (*n*=553), but did not substantially enhance the coverage of typical EV proteins (**Fig. 1H** and **Data File S1**). High-resolution isoelectric focusing (HiRIEF) fractionation and tandem mass tag (TMT) LC-MS/MS of plEVs further increased the number of overlapping protein identities with gcEVs (*n*=772; **Fig. 1H**) and, more importantly, revealed the presence of several established EV markers, including tetraspannins

(*e.g.* CD81, CD9, CD63), annexins, RABs, heat shock, and ESCRT proteins (**Table S1** and **Data File S1**) (24, 25). Functional pathway analyses showed the enrichment for several pathways implicated in glioma biology, *e.g.* EGFR and integrin mediated signaling and angiogenesis (**Fig. S1A**). We conclude that SEC-based separation and high resolution MS/MS allowed the identification of several EV proteins previously unidentified by LC-MS/MS in complex samples such as plEVs (19), supporting the feasibility for downstream analyses.

Identification of syndecan-1 by targeted analysis of glioma patient plEVs

To explore plEVs as a minimally invasive tool for the discrimination between high grade and low grade gliomas, we applied the SEC protocol on plasma collected within a population-based, clinical study cohort encompassing consecutive patients referred to the neurosurgery department with a suspected brain tumor lesion (n=136). In this cohort, 69 were diagnosed with high grade (WHO IV) GBM and 17 with low grade (WHO II) astrocytoma (hereafter referred to as low grade glioma, LGG), as determined by surgery and histopathological examination according to clinical routine (**Fig. S1B**). Base-line (pre-operative) plasma samples were available from all LGG patients and 65 out of 69 GBM patients (in total n=82; patient characteristics are presented in **Data File S2**) that were included for SEC separation and further processing. The representativeness of the present cohort was determined by a relative survival of GBM *vs* LGG patients (HR: 0.21; 95% CI: 0.12-0.36; P<0.001; **Fig. S2A**) that was comparable with data from The Cancer Genome Atlas (TCGA) cohort encompassing 850 patients (HR: 0.17; 95% CI: 0.14-0.19; P<0.001; **Fig. S2B**). PlEVs were isolated from all patients by SEC and analyzed employing an ultrasensitive immunoassay based on proximity extension assay (PEA) technology (**Fig. 2A**) (26, 27). The multiplex format allowed the simultaneous analysis of 183 proteins that were selected based on their known involvement in glioma biology and potential sorting to EVs (**Table S2**). Half of the analyzed proteins (n=92)

were above limit of detection in at least 20% of the samples. Using linear regression and adjusting for age (there was no gender difference between GBM and LGG groups), in total 12 plEV-associated proteins significantly differed between GBM and LGG (P<0.05), half of which were detectable in at least 98% of plEV samples (**Fig. 2B**). When adjusting for multiple testing, specifically syndecan-1 (SDC1) differed significantly between GBM and LGG (**Fig. 2C**) whereas integrin beta chain-2 (ITGB2) showed a strong trend, however not significant (**Fig. 2D**). Notably, SDC1 and ITGB2 are single-pass type I membrane proteins, which identifies them as potential EV surface biomarkers. To explore the diagnostic accuracy of plEV, receiver operating characteristic (ROC) curves were established. The ROC analysis revealed that plasma EV-SDC1 ($plEV^{SDC1}$) could discriminate patients with GBM from LGG, with an area under the curve (AUC) value of 0.81 (95% CI: 0.69-0.93) (**Fig. 2E**), and a sensitivity of 71% (95% CI: 44-89%) and specificity of 91% (95% CI: 81-97%). For plasma EV-ITGB2 ($plEV^{ITGB2}$) AUC was 0.77 (95% CI: 0.65-0.88) (**Fig. 2F**) with a sensitivity of 65% (95% CI: 38-86%) and specificity of 71% (95% CI: 58-81%).

Syndecan-1 tumor expression discriminates between GBM and LGG

Interestingly, SDC1 and ITGB2 tumor mRNA expression data retrieved from the TCGA cohort (n=850) revealed that both transcripts were significantly higher in GBM as compared with LGG tumors (**Fig. 3A** and **Fig. S2C**). ROC analysis of SDC1 mRNA showed an AUC of 0.91 (95% CI: 0.89-0.93) (**Fig. 3B**) with a sensitivity of 79% (95% CI: 75-82%) and specificity of 91% (95% CI: 87-94%). For ITGB2, AUC was 0.76 (95% CI: 0.72-0.79) (**Fig. S2D**) with a sensitivity of 70% (95% CI: 66-74%) and specificity of 67% (95% CI: 59-74%). Moreover, high SDC1 expression was associated with wild type isocitrate dehydrogenase (IDH) typically found in primary GBM (**Fig. 3C**), and the mesenchymal GBM subtype (28) (**Fig. 3D**), and correlated with a more aggressive tumor phenotype, as supported by an

association between high SDC1 expression and worse patient outcome (**Fig. 3E**; high *vs* low SDC1; HR: 0.66; $P<0.05$). However, there was no significant association between tumor ITGB2 and GBM patient outcome (**Fig. S2E**; $P=0.24$). These gene expression data from a large, independent glioma cohort data thus corroborated our findings from proteomic analyses of plEVs (**Fig. 2**). We conclude that $plEV^{SDC1}$ as well as tumor SDC1 mRNA can discriminate between GBM and LGG, and correlate with GBM aggressiveness.

Syndecan-1 expression correlates with a hypoxic and pro-angiogenic phenotype

In accordance with its association to the mesenchymal GBM subtype, SDC1 expression correlated with several components involved in stroma remodeling and angiogenesis (**Fig. 3F** and **Fig. S3A**). SDC1 further correlated with molecules known to be hypoxia-induced (29), which was corroborated in GBM cells *in vitro* by gene array analyses (**Fig. S3B**). EVs derived from GBM cells have shown potent pro-angiogenic effects (11), especially when derived from hypoxic conditions (10). Accordingly, in pilot studies we could show that plEVs from GBM patients (SDC1-positive, as determined by ELISA; $n=3$) were significantly more potent at stimulating primary human brain microendothelial cell (HBMEC) migration as compared with plEVs from healthy subjects (SDC1-negative; $n=3$) (**Fig. 3G**). We conclude that SDC1 tumor expression associates with glioma grade and characteristics typical of GBM aggressiveness.

Syndecan-1 is sorted to GBM patient plEVs and GBM cell-derived EVs

The identification of SDC1 in plEVs was of particular interest given its suggested functional role in GBM (30-32) and other malignancies (33), and its key role in EV biogenesis and release as part of the SDC1-syntenin-ALIX pathway (34). Immunofluorescence staining for SDC1 in U3034 primary GBM cells (35) visualized a cytoplasmic, vesicular as well plasma

membrane distribution (**Fig. 4A**). The vesicular localization of SDC1 was corroborated by co-staining experiments for SDC1 and vesicle markers, showing co-localization of SDC1 with the endosomal marker EEA1 and the late endosome/lysosomal and EV marker CD63 (**Fig. S4A)**. A similar distribution of SDC1 was found in GBM patient tumors (**Fig. 4B**), while SDC1 was not detected in normal brain tissue (**Fig. 4C**). Further, SDC1 was efficiently sorted to the EV fraction while undetectable in the soluble fraction in culture media from primary (**Fig. 4D**) as well as established (**Fig. 4E**) GBM cells. Notably, low density lipoprotein (LDL), a common contaminant of plEV preparations (19, 20), was negative for SDC1 (**Fig. S4B**). We next performed electron microscopy (EM) studies of plEVs isolated from GBM patients and gcEVs from GBM cell medium. Both EV sources showed positive labelling for SDC1 **(Fig. 4F** and **Fig. S4C**). We conclude that SDC1 is efficiently sorted to GBM-derived EVs, and provide evidence that SDC1 is associated with plEVs isolated from GBM patients.

PlEV^{SDC1} correlates with glioma grade and tumor SDC1 protein expression

We next sought to validate plEV^{SDC1} data from the glioma PEA cohort by a quantitative immunoassay. Interestingly, ELISA-based quantification of plEV^{SDC1} could discriminate between GBM and LGG patients with a higher significance level (P=0.0002; **Fig. 5A**) as compared with the PEA-based analysis (P=0.0498; **Fig. 2C**). ELISA appeared less sensitive than PEA with 13% (8 out of 61), 65% (11 out of 17), and 100% (4 out of 4) samples below detection level in GBM, LGG, and healthy controls, respectively. ROC analysis showed an AUC of 0.82 (95% CI: 0.71-0.93) (**Fig. 5B**) with a sensitivity of 71% (95% CI: 0.44-0.89%) and specificity of 80% (95% CI: 68-89%). In concordance with the TCGA data (**Fig. 3C**), we found a significant correlation between plEV^{SDC1} and IDH status, *i.e.* high plEV^{SDC1}was associated with wild type IDH (**Fig. S2F**). Further, the association between plEV^{SDC1} and GBM patient survival (high *vs* low plEV^{SDC1}; HR: 0.61; P<0.05; **Fig. 5C**) was similar to

SDC1 survival data in TCGA patients (high *vs* low SDC1; HR: 0.66; $P<0.05$; **Fig. 3E**), thus providing indirect support that plEV^{SDC1} levels reflect tumor SDC1 expression. To investigate this more directly, matched tumors from patients with low, moderate, and high plEV^{SDC1} were analyzed for SDC1 expression by immunohistochemistry. Importantly, SDC1 expression in paired plEV and tumor samples closely correlated; we observed virtually no staining in plEV^{SDC1} low patients, and limited and strong signal in tumors from patients with moderate and high plEV^{SDC1} levels, respectively (**Fig. 5D**). To further investigate how plEV^{SDC1} levels correlate with tumor status, we evaluated plEV^{SDC1} of GBM patients pre-operatively and post-operative day 21 prior to start of oncological treatment (n=15). Overall, the results showed a significant decrease in plEV^{SDC1} following surgery (**Fig. 6A**). However, this analysis also revealed interindividual variations; in addition to the patients showing decreasing plEV^{SDC1} levels (n=10), 2 patients had unchanged plEV^{SDC1} and 3 patients showed increased plEV^{SDC1} (**Fig. 6A**). We hypothesized that this reflects differences in the extent of surgery that ranged from biopsy to complete resection. To test this possibility, we analyzed available magnetic resonance imaging (MRI) data, revealing that patients that had a total or subtotal resection also showed a post-operative decline in plEV^{SDC1} (**Fig. 6B**). On the contrary, MRI data from patients with unaltered or even increased post-operative plEV^{SDC1} showed remaining contrast enhancement following surgery (**Fig. 6C**). We conclude that glioma tumors release plEV^{SDC1} into the circulation depending on their histologic grade, aggressiveness, and extent of surgical removal.

Discussion

We report the establishment of a procedure for the isolation of plEVs combined with targeted analyses of almost 200 proteins using ultrasensitive immunodetection technology, and identify SDC1 as a plEV constituent for non-invasive differentiation between GBM and LGG. SDC1 tumor expression similarly discriminated between GBM and LGG in a large glioma patient population from the TCGA cohort. Importantly, tumor-derived EVs remain a rarity in clinical samples, *i.e.* it was essential to elucidate how plEV^{SDC1} correlates with tumor SDC1. We find strong support of plEV^{SDC1} originating from GBM tumors by analyses of SDC1 expression in matched patient tumor specimens as well as in longitudinal (pre- and post-operative) plEV isolates. Together, our results provide important support to the concept of EV proteomics for non-invasive brain tumor diagnosis. In addition, we provide new insights into the role of SDC1 in glioma biology.

The attractiveness of EVs as a circulating biomarker relies on their relative structural robustness as compared with free nucleic acids and circulating tumor cells that may have limited use in glioma diagnosis due to *e.g.* poor passage over the blood brain barrier and a glial cell origin. Apart from in GBM, considerable interest has recently been focused on EV-based approaches in pancreatic ductal adenocarcinoma (PDAC) (36), including a recent study (37) that identified a signature of five plEV proteins to diagnose PDAC with an AUC of 0.84 and a sensitivity and specificity of 86% and 81%, respectively (n=43). As a comparison, we find that plEV^{SDC1}, *i.e.* a single marker, can discriminate between GBM and LGG with an AUC of 0.82 and a sensitivity and specificity of 71% and 80%, respectively (n=82). This can be compared with MRI, which is the currently used standard modality in the diagnosis and prognosis of brain tumors. The discrimination between GBM and LGG is based primarily on gadolinium (Gd) enhancement (a marker of blood-brain-barrier disruption). However, it can still be a challenge in clinical practice as high grade tumors may demonstrate no Gd

enhancement, while low grade tumors occasionally do. Accordingly, diagnostics by conventional MRI has shown a sensitivity and specificity of approximately 70%. Perfusion MRI and MR spectroscopy may improve the accuracy in discriminating between HGG and LGG tumors, but has not been implemented for pre-operative, diagnostic purposes (38, 39). Notably, most previous studies apply differential centrifugation to isolate EVs from plasma; even highly sensitive approaches using *e.g.* micro-fluidic chip technology (14) and advanced nanoplasmonic sensing systems (37) were preceded by ultracentrifugation that may largely influence the integrity and contents of EVs for downstream analyses. Further, time-consuming centrifugation procedures are practically incompatible with future clinical protocols. SEC has recently emerged as the "gold standard" to yield purified EVs from complex biological samples (19, 22-24, 40-42). For experimental consistency and reproducibility, we employed a standardized, commercially available column based on a Sephadex resin of approximately 75 nm pore size. Using the same SEC procedure, others similarly found that the purest EV pool is contained up to fractions 9, and that the bulk of plasma proteins will elute in later fractions (19, 22). In fact, typical EV markers, such as CD9, CD63, and CD81 have previously been identified in plEVs with western blot, electron microscopy, or flow cytometry, however, with LC-MS/MS only by a recent study using a similar SEC protocol combined with density cushion ultracentrifugation (19).

SDC1 has a well-established role as a growth factor and lipoprotein co-receptor during tumor development, and is overexpressed in myeloma and in epithelial tumors of various origins, including in breast cancer (33, 43, 44). In line with our findings, SDC1 mRNA was non-detectable in normal brain while expressed in several GBM cell-lines (30), and the survival rate was lower in patients with SDC1 positive as compared with SDC1 negative tumors (31). SDC1 expression has been found to be low in most normal tissues and, accordingly, systemic treatment with the indatuximab-ravtansine antibody-drug conjugate targeted at SDC1 was

well tolerated in a I/IIa trial with myeloma patients (45). However, SDC1 is expressed in epithelial cells of *e.g.* the skin and gastrointestinal tract (46), and can be shed as a soluble component into plasma (47). The increased secretion of $plEV^{SDC1}$ by GBM tumors may relate to the direct role of SDC1 in EV biogenesis as part of a machinery involving syntenin and heparanase, *i.e.* proteins implicated in GBM pathogenesis (48, 49). Interestingly, we found other important promotors of EV biogenesis, RAB27A and ARF6 (50, 51), to be correlated with SDC1 in GBM (**Fig. 3F**), which may also contribute to the excessive release of $plEV^{SDC1}$ from GBM tumors. Future studies should determine whether these independent observations are causally connected, *i.e.* if SDC1-mediated induction of the EV release pathway confers a more aggressive tumor phenotype in glioma. If so, SDC1 would appear as an interesting target for perturbation of the EV machinery, and $plEV^{SDC1}$ as an attractive biomarker of any such intervention.

Although the identification of $plEV^{SDC1}$ provides important proof-of-principle, this study has limitations. The current study was designed as a feasibility study, and needs to be corroborated in expanded clinical cohorts to also include other types of brain lesions that can be challenging to differentiate by MRI. Future studies should aim at identifying additional EV membrane markers that can be utilized for the enrichment of tumor-derived EVs. This may require a more comprehensive approach, as encouraged by our pilot studies employing advanced LC-MS/MS during optimization of the SEC procedure. We found hundreds of proteins in plEVs that overlapped with GBM cell-derived EVs, several of which are established EV membrane markers.

In summary, we identify $plEV^{SDC1}$ as a potential tool to facilitate non-invasive diagnosis of gliomas. Our results provide important support to the concept of EVs as a circulating "miniature of its cell of origin", and further motivate the future development of high through-

put, quantitative LC-MS/MS procedures to take full advantage of EVs as liquid biopsy biomarkers in cancer.

Acknowledgments

We thank all the patients and their families who participated in the study, and all the investigators and staff who contributed their time and effort to this study. We also thank Anna Weddig, research nurse, for help with the collection and handling of patient samples, and the Uppsala University Human Glioma Cell Culture resource (HGCC, www.hgcc.se) for sharing U3034 cells.

References

1. Louis DN, Perry A, Reifenberger G, von Deimling A, Figarella-Branger D, Cavenee WK *et al*. The 2016 World Health Organization Classification of Tumors of the Central Nervous System: a summary. *Acta Neuropathol* **2016**; 131(6):803-820.
2. Omuro A, DeAngelis LM. Glioblastoma and other malignant gliomas: a clinical review. *Jama* **2013**; 310(17):1842-1850.
3. Westphal M, Lamszus K. Circulating biomarkers for gliomas. *Nat Rev Neurol* **2015**; 11(10):556-566.
4. Tkach M, Thery C. Communication by Extracellular Vesicles: Where We Are and Where We Need to Go. *Cell* **2016**; 164(6):1226-1232.
5. Becker A, Thakur BK, Weiss JM, Kim HS, Peinado H, Lyden D. Extracellular Vesicles in Cancer: Cell-to-Cell Mediators of Metastasis. *Cancer Cell* **2016**; 30(6):836-848.
6. Maas SLN, Breakefield XO, Weaver AM. Extracellular Vesicles: Unique Intercellular Delivery Vehicles. *Trends Cell Biol* **2017**; 27(3):172-188.
7. Nakano I, Garnier D, Minata M, Rak J. Extracellular vesicles in the biology of brain tumour stem cells--Implications for inter-cellular communication, therapy and biomarker development. *Semin Cell Dev Biol* **2015**; 40:17-26.
8. Théry C. Diagnosis by extracellular vesicles. *Nature* **2015**; 523:161.
9. Xu R, Rai A, Chen M, Suwakulsiri W, Greening DW, Simpson RJ. Extracellular vesicles in cancer — implications for future improvements in cancer care. *Nat Rev Clin Oncol* **2018**.
10. Kucharzewska P, Christianson HC, Welch JE, Svensson KJ, Fredlund E, Ringner M *et al*. Exosomes reflect the hypoxic status of glioma cells and mediate hypoxia-

dependent activation of vascular cells during tumor development. *Proc Natl Acad Sci U S A* **2013**; 110(18):7312-7317.

11. Skog J, Wurdinger T, van Rijn S, Meijer D, Gainche L, Sena-Esteves M *et al*. Glioblastoma microvesicles transport RNA and protein that promote tumor growth and provide diagnostic biomarkers. *Nat Cell Biol* **2008**; 10(12):1470-1476.
12. Ricklefs FL, Alayo Q, Krenzlin H, Mahmoud AB, Speranza MC, Nakashima H *et al*. Immune evasion mediated by PD-L1 on glioblastoma-derived extracellular vesicles. *Science Advances* **2018**; 4(3).
13. Figueroa JM, Skog J, Akers J, Li H, Komotar R, Jensen R *et al*. Detection of wild-type EGFR amplification and EGFRvIII mutation in CSF-derived extracellular vesicles of glioblastoma patients. *Neuro Oncol* **2017**; 19(11):1494-1502.
14. Shao H, Chung J, Balaj L, Charest A, Bigner DD, Carter BS *et al*. Protein typing of circulating microvesicles allows real-time monitoring of glioblastoma therapy. *Nat Med* **2012**; 18(12):1835-1840.
15. Shao H, Chung J, Lee K, Balaj L, Min C, Carter BS *et al*. Chip-based analysis of exosomal mRNA mediating drug resistance in glioblastoma. *Nat Commun* **2015**; 6:6999.
16. Chen WW, Balaj L, Liau LM, Samuels ML, Kotsopoulos SK, Maguire CA *et al*. BEAMing and Droplet Digital PCR Analysis of Mutant IDH1 mRNA in Glioma Patient Serum and Cerebrospinal Fluid Extracellular Vesicles. *Mol Ther Nucleic Acids* **2013**; 2:e109.
17. Noerholm M, Balaj L, Limperg T, Salehi A, Zhu LD, Hochberg FH *et al*. RNA expression patterns in serum microvesicles from patients with glioblastoma multiforme and controls. *BMC Cancer* **2012**; 12(1):22.

18. Balaj L, Lessard R, Dai L, Cho Y-J, Pomeroy SL, Breakefield XO *et al*. Tumour microvesicles contain retrotransposon elements and amplified oncogene sequences. *Nat Commun* **2011**; 2:180-180.

19. Karimi N, Cvjetkovic A, Jang SC, Crescitelli R, Hosseinpour Feizi MA, Nieuwland R *et al*. Detailed analysis of the plasma extracellular vesicle proteome after separation from lipoproteins. *Cell Mol Life Sci* **2018**; 75(15):2873-2886.

20. Sódar BW, Kittel Á, Pálóczi K, Vukman KV, Osteikoetxea X, Szabó-Taylor K *et al*. Low-density lipoprotein mimics blood plasma-derived exosomes and microvesicles during isolation and detection. *Sci Rep* **2016**; 6:24316.

21. Thery C, Amigorena S, Raposo G, Clayton A. Isolation and characterization of exosomes from cell culture supernatants and biological fluids. *Curr Protoc Cell Biol* **2006**; Chapter 3:Unit 3.22.

22. Böing AN, van der Pol E, Grootemaat AE, Coumans FAW, Sturk A, Nieuwland R. Single-step isolation of extracellular vesicles by size-exclusion chromatography. *J Extracell Vesicles* **2014**; 3:10.3402/jev.v3403.23430.

23. Welton JL, Webber JP, Botos L-A, Jones M, Clayton A. Ready-made chromatography columns for extracellular vesicle isolation from plasma. *J Extracell Vesicles* **2015**; 4:10.3402/jev.v3404.27269.

24. Kowal J, Arras G, Colombo M, Jouve M, Morath JP, Primdal-Bengtson B *et al*. Proteomic comparison defines novel markers to characterize heterogeneous populations of extracellular vesicle subtypes. *Proc Natl Acad Sci U S A* **2016**; 113(8):E968-977.

25. Keerthikumar S, Chisanga D, Ariyaratne D, Al Saffar H, Anand S, Zhao K *et al*. ExoCarta: A Web-Based Compendium of Exosomal Cargo. *J Mol Biol* **2016**; 428(4):688-692.

26. Enroth S, Johansson Å, Enroth SB, Gyllensten U. Strong effects of genetic and lifestyle factors on biomarker variation and use of personalized cutoffs. *Nat Commun* **2014**; 5:4684.

27. Larssen P, Wik L, Czarnewski P, Eldh M, Lof L, Ronquist KG *et al*. Tracing Cellular Origin of Human Exosomes Using Multiplex Proximity Extension Assays. *Mol Cell Proteomics* **2017**; 16(3):502-511.

28. Verhaak RGW, Hoadley KA, Purdom E, Wang V, Qi Y, Wilkerson MD *et al*. An integrated genomic analysis identifies clinically relevant subtypes of glioblastoma characterized by abnormalities in PDGFRA, IDH1, EGFR and NF1. *Cancer cell* **2010**; 17(1):98.

29. Gilkes DM, Semenza GL, Wirtz D. Hypoxia and the extracellular matrix: drivers of tumour metastasis. *Nat Rev Cancer* **2014**; 14(6):430-439.

30. Watanabe A, Mabuchi T, Satoh E, Furuya K, Zhang L, Maeda S *et al*. Expression of syndecans, a heparan sulfate proteoglycan, in malignant gliomas: participation of nuclear factor-kappaB in upregulation of syndecan-1 expression. *J Neurooncol* **2006**; 77(1):25-32.

31. Xu Y, Yuan J, Zhang Z, Lin L, Xu S. Syndecan-1 expression in human glioma is correlated with advanced tumor progression and poor prognosis. *Mol Biol Rep* **2012**; 39(9):8979-8985.

32. Chen J, Tang J, Chen W, Gao Y, He Y, Zhang Q *et al*. Effects of syndecan-1 on the expression of syntenin and the migration of U251 glioma cells. *Oncol Lett* **2017**; 14(6):7217-7224.

33. Couchman JR. Syndecans: proteoglycan regulators of cell-surface microdomains? *Nat Rev Mol Cell Biol* **2003**; 4(12):926-937.

34. Baietti MF, Zhang Z, Mortier E, Melchior A, Degeest G, Geeraerts A *et al*. Syndecan-syntenin-ALIX regulates the biogenesis of exosomes. *Nat Cell Biol* **2012**; 14(7):677-685.

35. Xie Y, Bergström T, Jiang Y, Johansson P, Marinescu VD, Lindberg N *et al*. The Human Glioblastoma Cell Culture Resource: Validated Cell Models Representing All Molecular Subtypes. *EBio Medicine* **2015**; 2(10):1351-1363.

36. Melo SA, Luecke LB, Kahlert C, Fernandez AF, Gammon ST, Kaye J *et al*. Glypican-1 identifies cancer exosomes and detects early pancreatic cancer. *Nature* **2015**; 523(7559):177-182.

37. Yang KS, Im H, Hong S, Pergolini I, Del Castillo AF, Wang R *et al*. Multiparametric plasma EV profiling facilitates diagnosis of pancreatic malignancy. *Sci Transl Med* **2017**; 9(391).

38. Scott JN, Brasher PM, Sevick RJ, Rewcastle NB, Forsyth PA. How often are nonenhancing supratentorial gliomas malignant? A population study. *Neurology* **2002**; 59(6):947-949.

39. Law M, Yang S, Wang H, Babb JS, Johnson G, Cha S *et al*. Glioma Grading: Sensitivity, Specificity, and Predictive Values of Perfusion MR Imaging and Proton MR Spectroscopic Imaging Compared with Conventional MR Imaging. *Am J Neuroradiol* **2003**; 24(10):1989-1998.

40. Gardiner C, Di Vizio D, Sahoo S, Thery C, Witwer KW, Wauben M *et al*. Techniques used for the isolation and characterization of extracellular vesicles: results of a worldwide survey. *J Extracell Vesicles* **2016**; 5:32945.

41. Gamez-Valero A, Monguio-Tortajada M, Carreras-Planella L, Franquesa M, Beyer K, Borras FE. Size-Exclusion Chromatography-based isolation minimally alters

Extracellular Vesicles' characteristics compared to precipitating agents. *Sci Rep* **2016**; 6:33641.

42. Kreimer S, Ivanov AR. Rapid Isolation of Extracellular Vesicles from Blood Plasma with Size-Exclusion Chromatography Followed by Mass Spectrometry-Based Proteomic Profiling. *Methods Mol Biol* **2017**; 1660:295-302.

43. Afratis NA, Nikitovic D, Multhaupt HA, Theocharis AD, Couchman JR, Karamanos NK. Syndecans - key regulators of cell signaling and biological functions. *FEBS J* **2017**; 284(1):27-41.

44. Menard JA, Christianson HC, Kucharzewska P, Bourseau-Guilmain E, Svensson KJ, Lindqvist E *et al*. Metastasis Stimulation by Hypoxia and Acidosis-Induced Extracellular Lipid Uptake Is Mediated by Proteoglycan-Dependent Endocytosis. *Cancer Res* **2016**; 76(16):4828-4840.

45. Heffner LT, Jagannath S, Zimmerman TM, Lee KP, Rosenblatt J, Lonial S *et al*. BT062, an Antibody-Drug Conjugate Directed Against CD138, Given Weekly for 3 Weeks in Each 4 Week Cycle: Safety and Further Evidence of Clinical Activity. *Blood* **2012**; 120(21):4042-4042.

46. Consortium G. The Genotype-Tissue Expression (GTEx) project. *Nat Genet* **2013**; 45(6):580-585.

47. Ramani VC, Purushothaman A, Stewart MD, Thompson CA, Vlodavsky I, Au JL *et al*. The heparanase/syndecan-1 axis in cancer: mechanisms and therapies. *FEBS J* **2013**; 280(10):2294-2306.

48. Kegelman TP, Das SK, Hu B, Bacolod MD, Fuller CE, Menezes ME *et al*. MDA-9/syntenin is a key regulator of glioma pathogenesis. *Neuro Oncol* **2014**; 16(1):50-61.

49. Kundu S, Xiong A, Spyrou A, Wicher G, Marinescu VD, Edqvist PD *et al*. Heparanase Promotes Glioma Progression and Is Inversely Correlated with Patient Survival. *Mol Cancer Res* **2016**; 14(12):1243-1253.

50. Ostrowski M, Carmo NB, Krumeich S, Fanget I, Raposo G, Savina A *et al*. Rab27a and Rab27b control different steps of the exosome secretion pathway. *Nat Cell Biol* **2010**; 12(1):19-30; sup pp 11-13.

51. Ghossoub R, Lembo F, Rubio A, Gaillard CB, Bouchet J, Vitale N *et al*. Syntenin-ALIX exosome biogenesis and budding into multivesicular bodies are controlled by ARF6 and PLD2. *Nat Commun* **2014**; 5:3477.

52. Mork M, Handberg A, Pedersen S, Jorgensen MM, Baek R, Nielsen MK *et al*. Prospects and limitations of antibody-mediated clearing of lipoproteins from blood plasma prior to nanoparticle tracking analysis of extracellular vesicles. *J Extracell Vesicles* **2017**; 6(1):1308779.

Figure Legends

Figure 1. Characterization of plasma EVs isolated by size exclusion chromatography. **(A)** Schematic representation of LC-MS/MS proteomic analysis of GBM cell EVs isolated by ultracentrifugation, and patient plasma EVs (plEVs) isolated by size exclusion chromatography (SEC). **(B)** Gel electrophoresis shows the bulk of plasma proteins in SEC fractions 10-15. M, Size marker. Nano tracking analysis shows that particle concentration peaks in SEC fraction 9 **(C)**, and comparable size distribution of EVs from cells **(D)** and plasma **(E)**. Electron microscopy shows comparable shape and size distribution of EVs from cells **(F)** and plasma **(G)**. Scale bar, 200 nm. (**H)** Venn diagram illustrating proteins identified in plEVs and cell-derived EVs using LC-MS/MS procedures as indicated. Data were compared with ExoCarta, a public EV proteomics database. NG, Normal gradient (n=22 for cell EVs and n=8 for plEVs); LG, Long gradient (n=8); TMT: Tandem Mass Tags; HiRIEF: High-resolution isoelectric focusing (n=10).

Figure 2. Identification of SDC1 and ITGB2 as candidate plasma EV proteins that differentiate between GBM and LGG. (A) Procedure for patient plasma EV (plEV) isolation and analysis by multiplex immunoassay based on proximity extension technology. (**B)** Summary of plEV protein levels in GBM vs LGG patients. "Missing values" shows fraction of total sample number below limit of detection. *P*-value was adjusted for multiple testing using Benjamini-Hochberg's correction method for controlling the false discovery rate (FDR) set at <5%. **(C)** Significantly increased $plEV^{SDC1}$ in GBM vs LGG patients after correction for multiple testing. **(D)** $PlEV^{ITGB2}$ levels in GBM did not significantly differ from LGG patients. Shown are adjusted P-values. NPX, Normalized Protein eXpression. Receiver

operating characteristic (ROC) curve was used to determine the accuracy of plEV^{SDC1} **(E)** and plEV^{ITGB2} **(F)** to discriminate between GBM and LGG. AUC, Area under the curve.

Figure 3. SDC1 tumor expression correlates with glioma grade and tumor aggressiveness. (A) SDC1 expression in GBM and LGG tumors. Shown is adjusted P-value. (**B**) ROC curve of SDC1 expression data from GBM and LGG patients. **(C)** SDC1 expression correlates with GBM IDH mutation status. **(D)** SDC1 expression correlates with mesenchymal GBM subtype. **(E)** SDC1 expression correlates with GBM patient outcome. Patients (*n*=160) were dichotomized according to median SDC1 expression level. **(F)** SDC1 correlates with factors involved in tumor stroma remodeling, hypoxia, angiogenesis, EV biogenesis and acidosis. **A-F**: Data were retrieved from the TCGA and GlioVis portals. **(G)** GBM patient-derived plEVs stimulate the migration of primary human brain microendothelial cells (HBMECs). Migration of HBMECs towards serum-free medium supplemented with plEVs (5 μg/ml) from healthy subjects (Control, negative for SDC1) or from GBM patients (positive for SDC1). Data are presented as the mean ± SD from three independent experiments (*n*=3 healthy subjects and GBM patients), each performed in triplicates. **P*< 0.05.

Figure 4. SDC1 protein expression in EVs, GBM primary cells and GBM patient tumors. (A) Immunofluorescence and high-resolution confocal microscopy imaging shows SDC1 (red) localization in plasma membrane and cytoplasmic vesicles in primary GBM cells. DAPI: Nuclear stain. Scale bar, 5 μm. **(B)** Immunohistochemistry shows SDC1 expression in the plasma membrane (upper panel) and cytoplasmic puncta (mid panel) of patient GBM tumor. **(C)** SDC1 was absent in normal brain. Scale bar, 50 μm. Primary human GBM U3034 cells **(D)** and established U87-MG cells **(E)** and their corresponding EVs and total

conditioned media (CM) were analyzed by immunoblotting demonstrating SDC1 sorting to the EV fraction. Equal amounts of total protein were analyzed for SDC1 and the EV marker TSG101 or flotillin 1 by Western blotting. **(F)** Electron microscopy of GBM patient plasma EVs stained with gold-conjugated secondary antibody only as control (left panel) or with primary anti-SDC1 and secondary antibody (right panel). Arrow indicates EV staining positive for SDC1. Scale bar, 100 nm.

Figure 5. Plasma EV SDC1 discriminates between GBM and LGG and correlates with tumor SDC1 expression. (A) Quantitative ELISA analysis of SDC1 levels in plasma EVs (plEV^{SDC1}) isolated from GBM and LGG patients. **(B)** ROC curve of plEV^{SDC1} in GBM and LGG patients. **(C)** PlEV^{SDC1} correlates with GBM patient outcome. **(D)** SDC1 expression in matched tumors from patients with low (upper panels), moderate (mid panels) and high (lower panels) plEV^{SDC1} levels. Shown are two representative tumors from each group at two different magnifications. Figures above images indicate plEV^{SDC1} levels (pg/ml) just prior to surgery. ND, not detected. Scale bars, 50 μm.

Figure 6. Plasma EV SDC1 in longitudinal samples reveals decreased levels post-operatively. (A) ELISA analysis of SDC1 levels in plasma EVs (plEV^{SDC1}) isolated from GBM patients either prior to (Pre-op) or 21 days after (Post-op) surgery shows an overall reduction post-operatively. Blue, red and black colors indicate decreased, increased and unchanged levels, respectively. **(B)** and **(C)** Change in plEV^{SDC1} appears to correlate with extent of surgery. Magnetic resonance imaging (MRI) performed pre-op and within 48 h after surgery (Post-op 48 h) shows complete resection (Patient #1), near complete resection (Patient #2), and subtotal resection (Patient #3) of contrast enhancing tumor tissue in GBM patients with a post-operative decrease in plEV^{SDC1} **(B)**. MRI shows status after biopsy (Patient #4),

partial resection (Patient #5), and subtotal resection (Patient #6) in patients with stable or increased post-operative $plEV^{SDC1}$ **(C)**. Figures above and below images indicate $plEV^{SDC1}$ levels (pg/ml) just prior to and 21 days after surgery, respectively, with same color coding as in **(A)**.

Figure 1
Author Manuscript Published OnlineFirst on January 24, 2019; DOI: 10.1158/1078-0432.CCR-18-2946
Author manuscripts have been peer reviewed and accepted for publication but have not yet been edited.

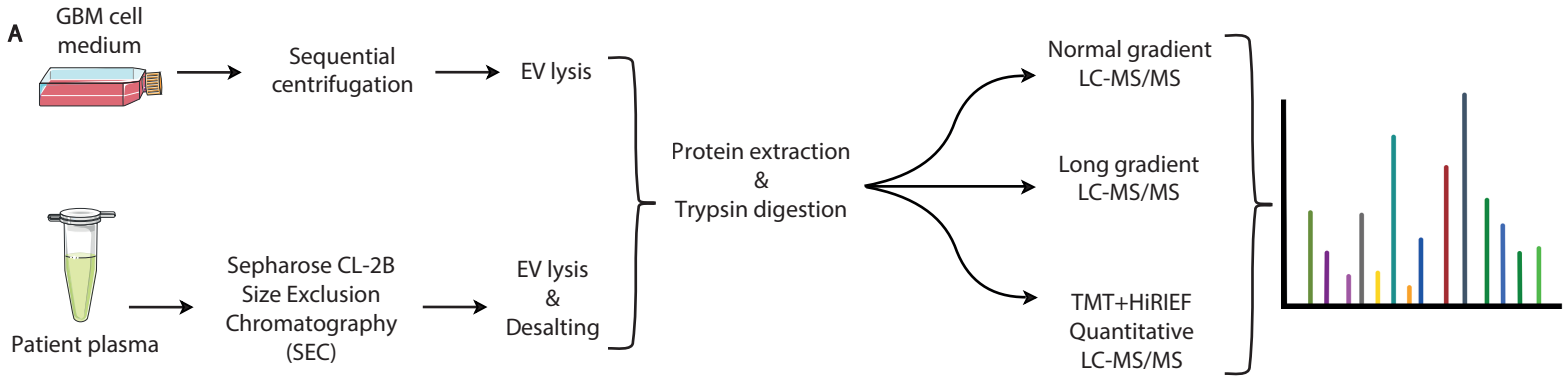

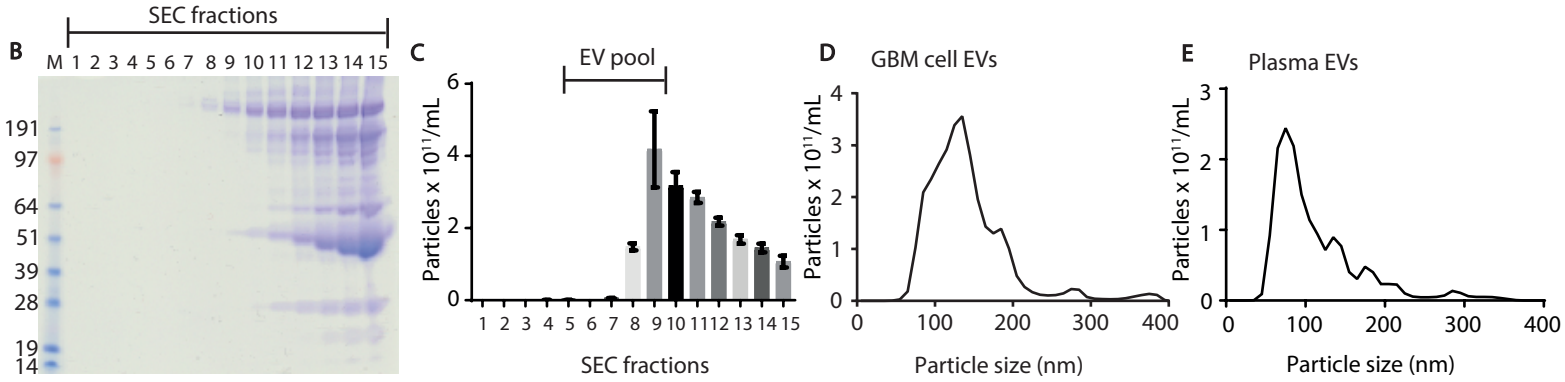

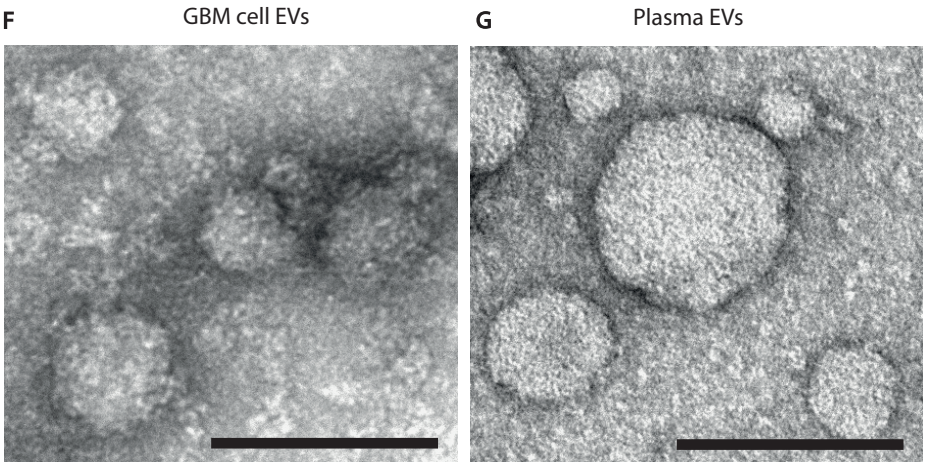

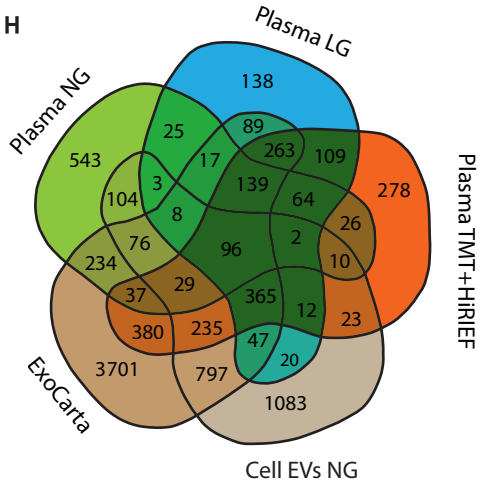

Figure 2

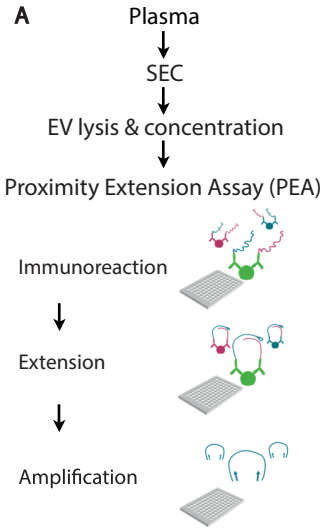

B

Protein ID	Missing values	Regression coefficient	P-value	Adjusted P-value
SDC1	0.01	0.96	0.0003	0.05
ITGB2	0.01	1.14	0.001	0.09
TR	0.37	2.13	0.004	0.19
PLC	0.35	2.02	0.005	0.19
CRNN	0.38	-2.21	0.008	0.25
Ep-CAM	0.27	1.89	0.01	0.26
AR	0.32	1.72	0.02	0.34
vWF	0.00	1.22	0.02	0.44
TRAIL	0.01	0.72	0.03	0.54
ADAM 8	0.01	0.51	0.05	0.57
CHI3L1	0.27	1.45	0.05	0.57
PRTN3	0.02	0.78	0.05	0.57

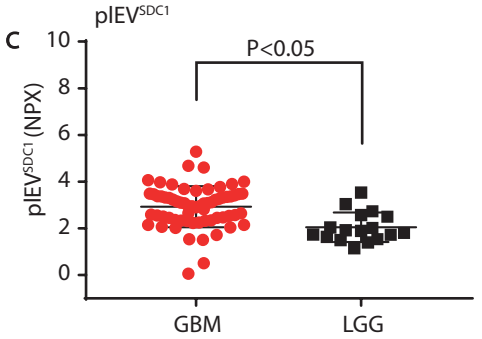

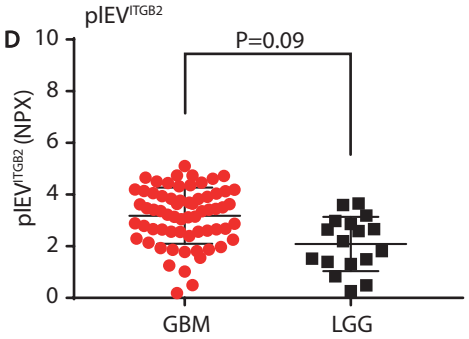

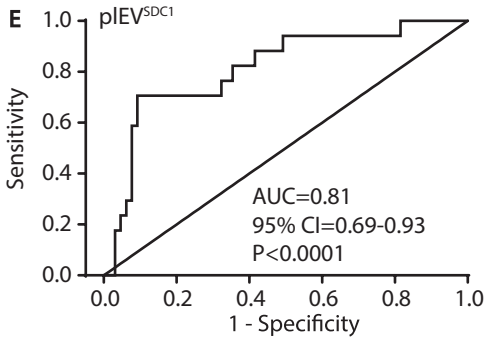

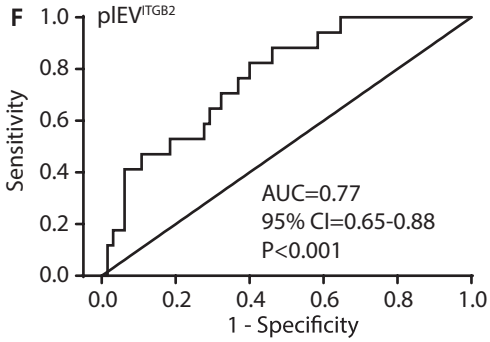

Author Manuscript Published OnlineFirst on January 24, 2019; DOI: 10.1158/1078-0432.CCR-18-2946
Author manuscripts have been peer reviewed and accepted for publication but have not yet been edited.

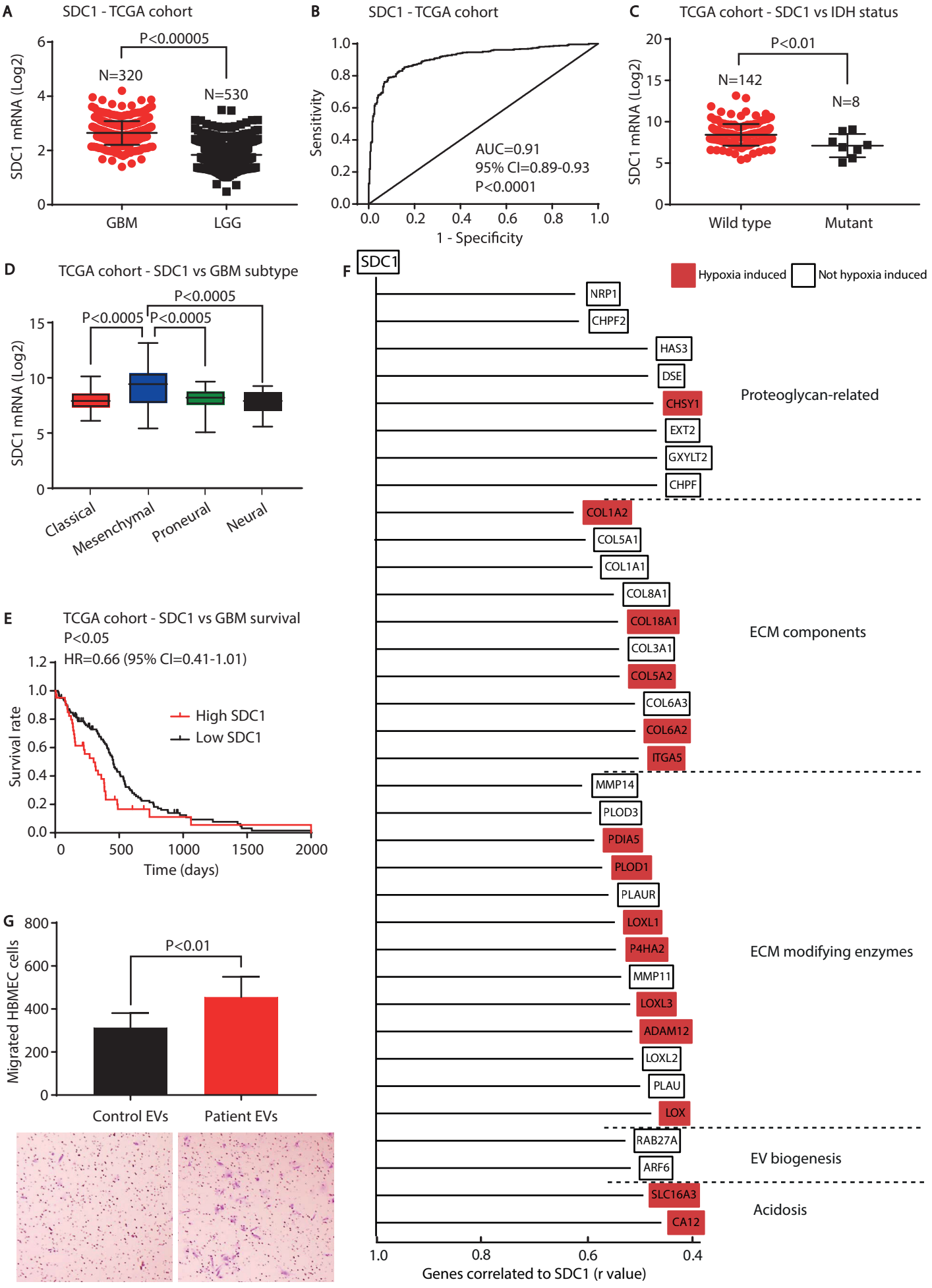

Figure 4

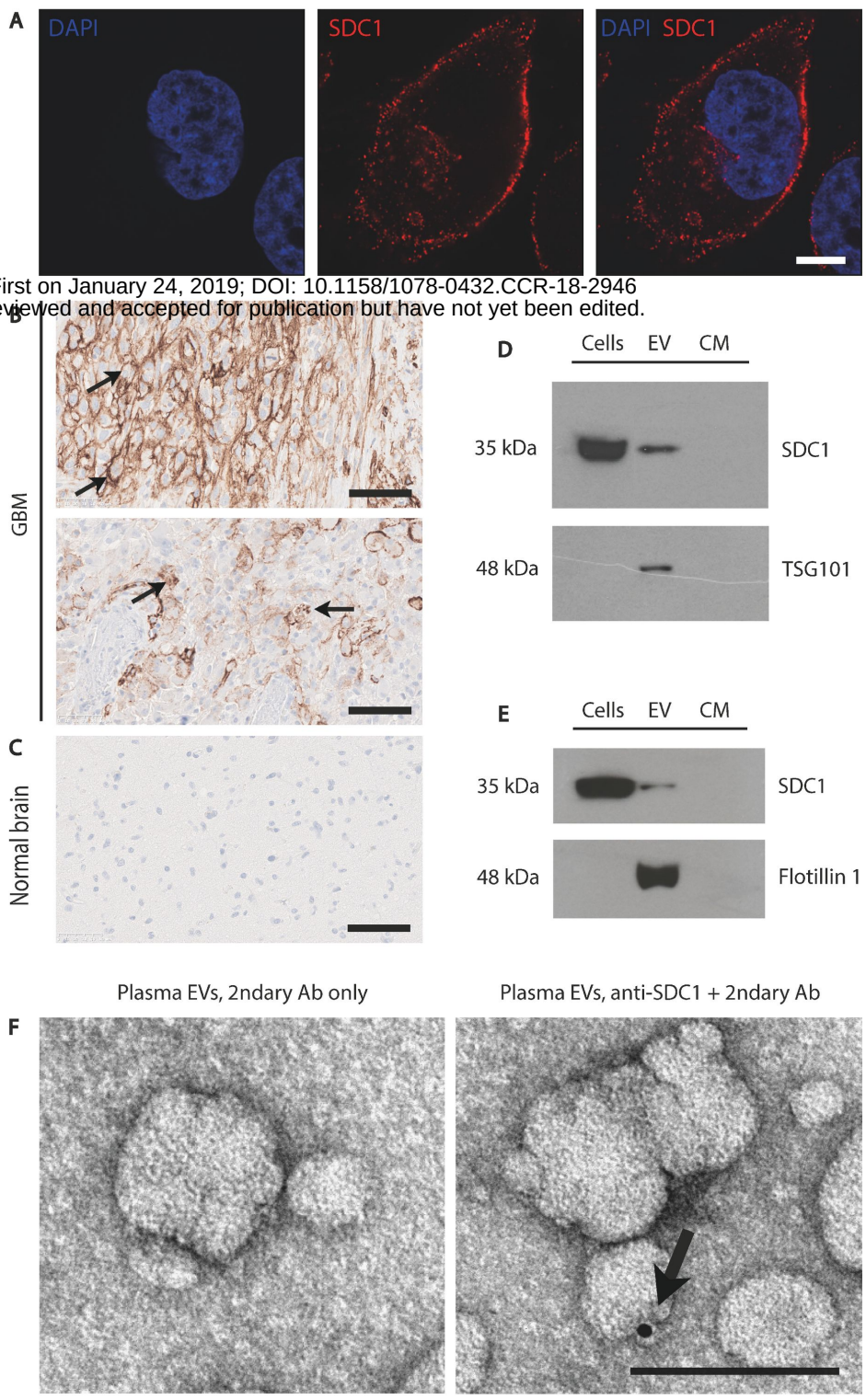

Figure 5

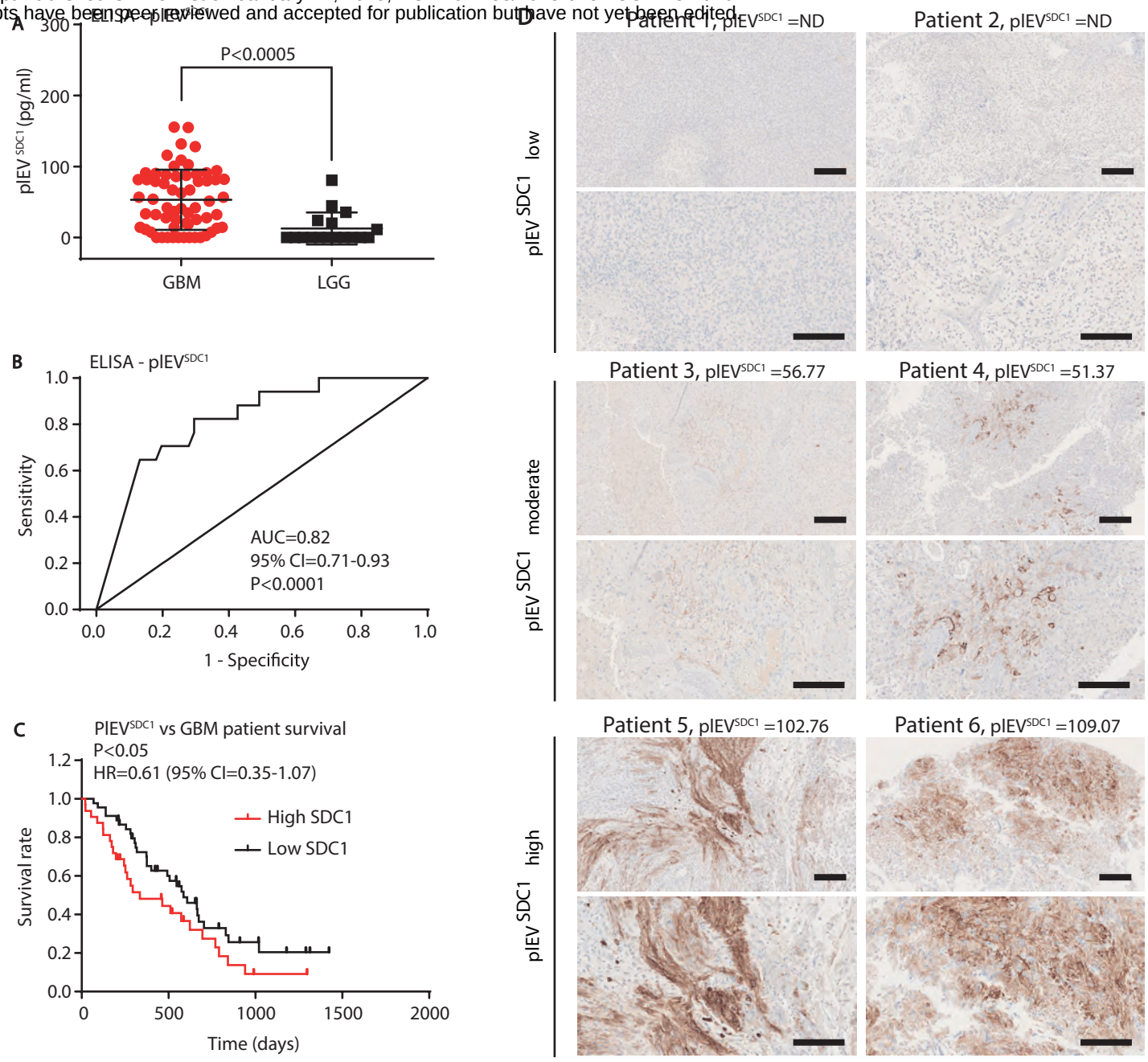

Figure 6

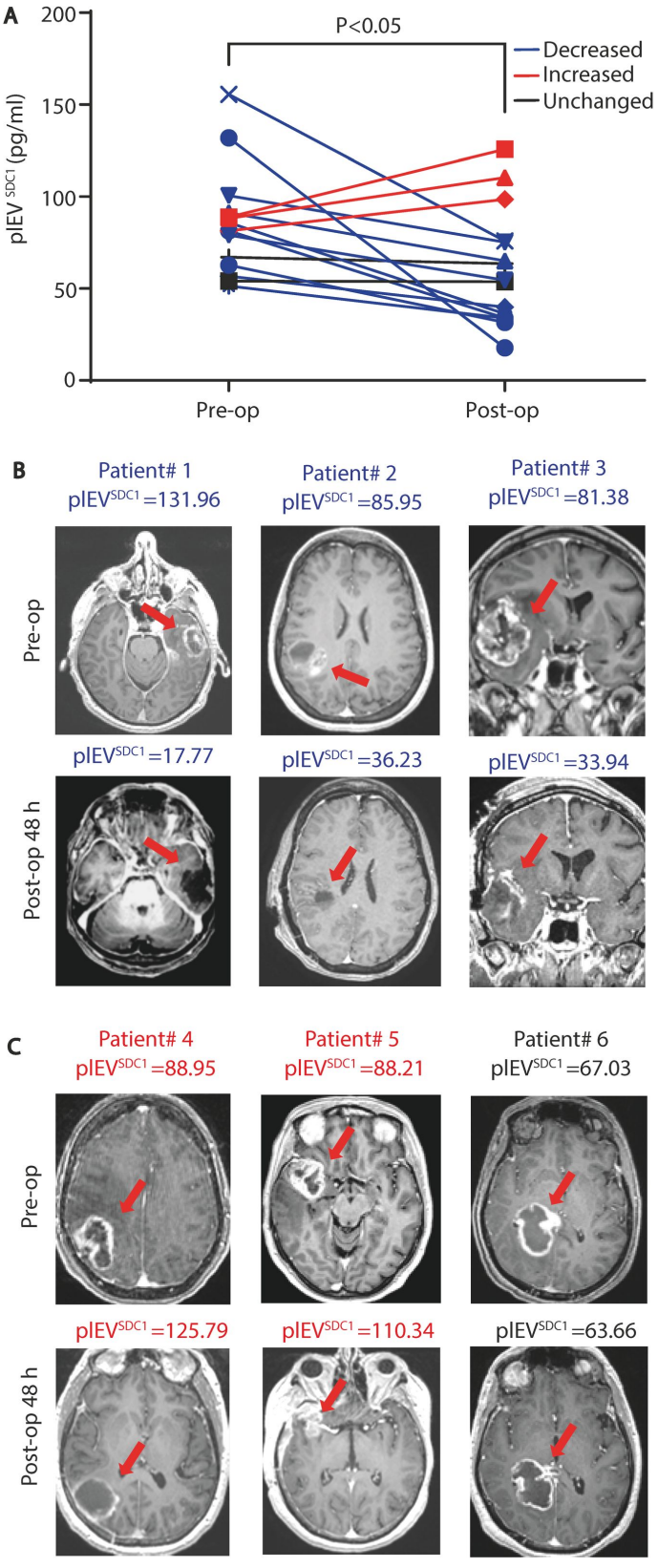

AACR American Association for Cancer Research

Clinical Cancer Research

Ultrasensitive immunoprofiling of plasma extracellular vesicles identifies syndecan-1 as a potential tool for minimally invasive diagnosis of glioma

Vineesh Indira Chandran, Charlotte Welinder, Ann-Sofie Månsson, et al.

Clin Cancer Res Published OnlineFirst January 24, 2019.